Electronic Supplementary Material (ESI) for Chemical Communications.
This journal is © The Royal Society of Chemistry 2023

Electronic Supplementary Information for

Zinc-dual-halide complexes suppressing polyhalide formation for rechargeable aqueous zinc-halogen batteries

Wanlong Wu, [a] Xiaoyu Yin, [a] Sibo Wang, [a] Quanwei Jiang, [a] Hua-Yu Shi [a] and Xiaoqi Sun [a,b,*]

[a] Department of Chemistry, Northeastern University, Shenyang 110819, China

[b] National Frontiers Science Center for Industrial Intelligence and Systems Optimization, Northeastern University, Shenyang 110819, China

*E-mail: sunxiaoqi@mail.neu.edu.cn

Experimental Section

Materials： Graphite foil was purchased from SGL group (Germany). Zinc foil, N-methylpyrrolidone (NMP), polyvinylidene difluoride (PVDF) and Super P was obtained from Sinopharm Chemical Reagent. Other reagents were purchased from Sinopharm Chemical Reagent Co., Ltd.

Preparation of cathode conductive medium: The cathode conductive medium was prepared by mixing Super P and PVDF at a mass ratio of 9:1 in NMP. The slurry was casted onto graphite foil and dried at 80°C for 12 hours. The mass loading of Super P and PVDF was around 3 mg cm^{-2}.

Material characterizations: Raman spectroscopy was conducted on BWS465-532S, B&W Tek Inc., USA with a 532 nm excitation laser. X-ray photoelectron spectroscopy (XPS) was carried out on KRATOS, Axis Ultra ^{DLD} with Al-Kα radiation (UK) as the excitation source. The data was analyzed using CasaXPS software and calibrated by referencing the C 1s peak to 284.6 eV. The electrodes for ex-situ Raman and XPS measurements were cycled 10 times for stabilization and charged/discharged to the desired states. In the Raman spectra, X_2 and polyhalide show apparent signals whereas halide ions do not. The electrodes were thus not washed for Raman analysis to retain and detect the possible signals from polyhalide. In the XPS spectra, on the other hand, halides also exhibit apparent signals. In order to eliminate halides from electrolytes, the electrodes were washed for XPS analysis.

Electrochemical measurements: Swagelok® type cells were assembled with Super P/PVDF cathode, Zn anode, and aqueous zinc halide electrolytes (100 uL). The areas of both electrodes were 1.13 cm^{-2}. Titanium rods were used as the current collectors. The current density and specific capacity were calculated based on the total mass of Super P and PVDF. Electrochemical impedance spectroscopy (EIS) measurements were carried out in the frequency range from 110 mHz to 100 kHz in three electrode cells with saturated calomel electrode (SCE) as the reference. The electrochemical measurements were performed on the Bio-logic VMP3 electrochemical system.

Computational details： Density functional theory (DFT) calculations were carried out with the Materials Studio 2019 software package. Geometrical optimizations were conducted at the Dmol3 basis set. Energy calculations were performed on the optimized structures.

Supporting figures and tables

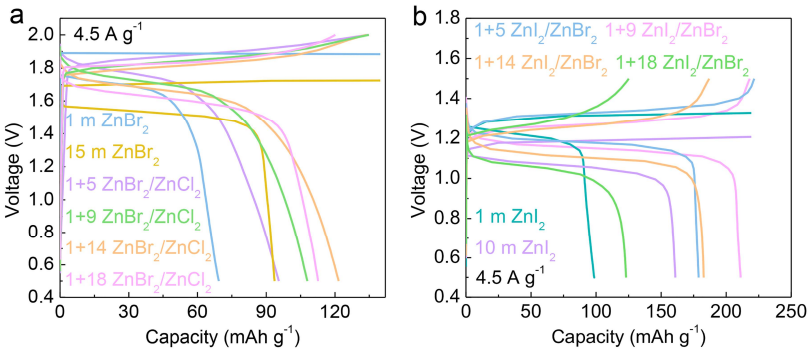

Fig. S1. Charge/discharge curves of a) Zn-Br_2 and b) Zn-I_2 cells at 4.5 A g^{-1} with different aqueous electrolytes. For the Zn-Br_2 cells, the coulombic efficiency increases with $ZnCl_2$ concentration, i.e., 49%, 67%, 71%, 80%, 91% and 94% obtained in the electrolytes of 1 m $ZnBr_2$, 15 m $ZnBr_2$, 1+5 $ZnBr_2/ZnCl_2$, 1+9 $ZnBr_2/ZnCl_2$, 1+14 $ZnBr_2/ZnCl_2$ and 1+18 $ZnBr_2/ZnCl_2$, respectively. Nevertheless, the capacity and overpotential in the 1+18 $ZnBr_2/ZnCl_2$ electrolyte are poorer than in 1+14 $ZnBr_2/ZnCl_2$. Similar trends are observed in the Zn-I_2 cells as well. By overall considerations of coulombic efficiency, capacity and overpotential, the 1+14 $ZnBr_2/ZnCl_2$ and 1+9 $ZnI_2/ZnBr_2$ appear to be optimal concentrations and are applied.

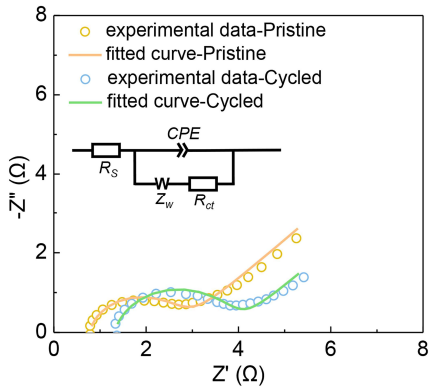

Fig. S2. The Nyquist plots and the fitted curves (inset showing the equivalent circuit) in the $ZnBr_2/ZnCl_2$ electrolyte.

Table S1. The fitted R_s and R_{ct} values in the $ZnBr_2/ZnCl_2$ electrolyte.

States	R_s (ohm)	R_{ct} (ohm)
Pristine	0.72	1.40
Cycled	0.96	1.92

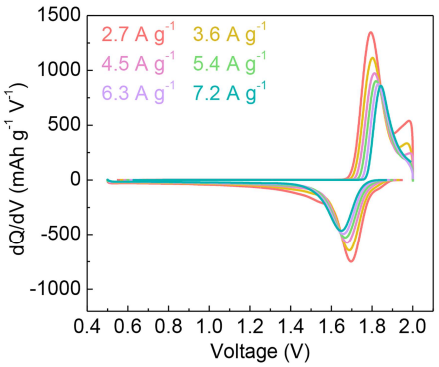

Fig. S3. The differential capacity curves at different current densities of Zn-Br_2 cells with the $ZnBr_2$/$ZnCl_2$ electrolyte.

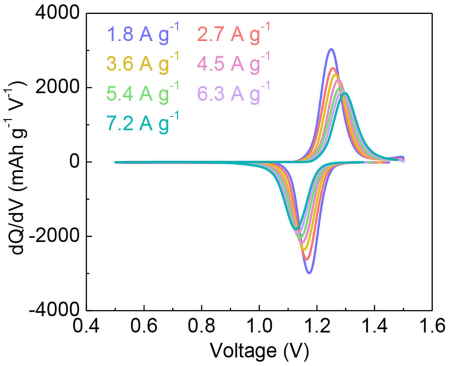

Fig. S4. The differential capacity curves at different current densities of Zn-I_2 cells with the ZnI_2/$ZnBr_2$ electrolyte.

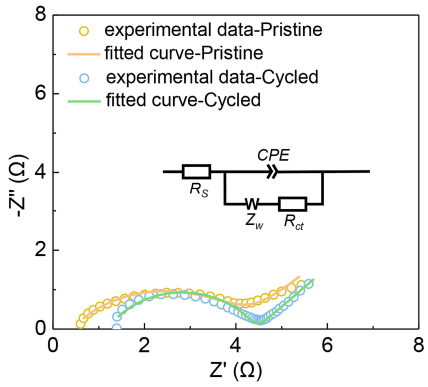

Fig. S5. The Nyquist plots and fitted curves (inset showing the equivalent circuit) in the ZnI_2/$ZnBr_2$ electrolyte.

Table S2. The fitted R_s and R_{ct} values in the ZnI_2/$ZnBr_2$ electrolyte.

States	R_s (ohm)	R_{ct} (ohm)
Pristine	0.39	4.46
Cycled	1.00	3.67

Table S3. Electrochemical performance comparison of the zinc-bromine battery with previous publications.

Cathode	Capacity	Cycling performance	CE	Ref.
AC@TBABr	98 mAh g^{-1}/1 A g^{-1}	Stable/2000/1 A g^{-1}	98%	[1]
Carbon Foam	36.8 mAh/20 mA	Stable/1000/20 mA	91%	[2]
Br_2-$Ti_3C_2T_X$	143 mAh g^{-1}/2 A g^{-1}	116 mAh g^{-1}/2000/2 A g^{-1}	97%	[3]
NGF-700	16 mAh/20 mA	Stable/1000/20 mA	85%	[4]
SP-PBH	1.85 mAh cm^{-2}/8 mA cm^{-2}	Stable/1200/8 mA cm^{-2}	92%	[5]
Super P	109 mAh g^{-1}/5.4 A g^{-1}	90 mAh g^{-1}/1200/5.4 A g^{-1}	92.7%	This work

Table S4. Electrochemical performance comparison of the zinc-iodine battery with previous publications.

Cathode	Capacity	Cycling performance	CE	Ref.
I_2@C	210 mAh g^{-1}/0.1 A g^{-1}	170 mAh g^{-1}/50/0.1 A g^{-1}	91.3%	[6]
NCCs/I_2	131 mAh g^{-1}/5 A g^{-1}	113 mAh g^{-1}/3500/5 A g^{-1}	~100%	[7]
Ketjen black	102.6 mAh g^{-1}/1.28 A g^{-1}	85.1 mAh g^{-1}/6000/1.92 A g^{-1}	99.65%	[8]
I_2@ACF	143 mAh g^{-1}/2C	128.7 mAh g^{-1}/3000/2C	~100%	[9]
I_2-C	300 mAh g^{-1}/2 mA cm^{-2}	275 mAh g^{-1}/200/2 mA cm^{-2}	99%	[10]
I_2-Co[$Co_xFe_{1-x}(CN)_6$]	236.8 mAh g^{-1}/0.1 A g^{-1}	165.6 mAh g^{-1}/2000/4 A g^{-1}	~100%	[11]
Carbon cloth	210 mAh g^{-1}/1C	198 mAh g^{-1}/500/1C	98.5%	[12]
I_2/OSTC	185 mAh g^{-1}/1 A g^{-1}	157.3 mAh g^{-1}/10000/1 A g^{-1}	~100%	[13]
NiSAs-HPC/I_2	188 mAh g^{-1}/5C	179 mAh g^{-1}/1000/5C	~100%	[14]
Carbon fiber paper	4.1 mAh cm^{-2}/0.3 mA cm^{-2}	stable/500/0.3 mA cm^{-2}	90%	[15]
Super P	204 mAh g^{-1}/5.4 A g^{-1}	198 mAh g^{-1}/2800/5.4 A g^{-1}	98%	This work

References

1. B. Evanko, S. J. Yoo, J. Lipton, S.-E. Chun, M. Moskovits, X. Ji, S. W. Boettcher and G. D. Stucky, *Energy Environ. Sci.,* 2018, **11**, 2865-2875.
2. S. Biswas, A. Senju, R. Mohr, T. Hodson, N. Karthikeyan, K. W. Knehr, A. G. Hsieh, X. Yang, B. E. Koel and D. A. Steingart, *Energy Environ. Sci.*, 2017, **10**, 114-120.
3. X. Li, N. Li, Z. Huang, Z. Chen, Y. Zhao, G. Liang, Q. Yang, M. Li, Q. Huang, B. Dong, J. Fan and C. Zhi, *ACS Nano,* 2021, **15**, 1718-1726.
4. J. H. Lee, Y. Byun, G. H. Jeong, C. Choi, J. Kwen, R. Kim, I. H. Kim, S. O. Kim and H. T. Kim, *Adv. Mater.,* 2019, **31**, 1904524.
5. W. Wu, S. Xu, Z. Lin, L. Lin, R. He and X. Sun, *Energy Storage Mater.*, 2022, **49**, 11-18.
6. W. Li, K. Wang and K. Jiang, *J. Mater. Chem. A,* 2020, **8**, 3785.
7. W. Liu, P. Liu, Y. Lyu, J. Wen, R. Hao, J. Zheng, K. Liu, Y. J. Li and S. Wang, *ACS Appl. Mater. Interfaces,* 2022, **14**, 8955-8962.
8. H. Yang, Y. Qiao, Z. Chang, H. Deng, P. He and H. Zhou, *Adv. Mater.*, 2020, **32**, 2004240.
9. H. Pan, B. Li, D. Mei, Z. Nie, Y. Shao, G. Li, X. S. Li, K. S. Han, K. T. Mueller and V. Sprenkle, *ACS Energy Lett.,* 2017, **2**, 2674-2680.
10. Y. Li, L. Liu, H. Li, F. Cheng and J. Chem, *Chem. Commun.,* 2018, **54**, 6792-6795.
11. L. Ma, Y. Ying, S. Chen, Z. Huang, X. Li, H. Huang and C. Zhi, *Angew. Chem. Int. Ed.,* 2021, **60**, 3791-3798.
12. K. K. Sonigara, J. Zhao, H. K. Machhi and G. Cui, *Adv. Energy Mater.,* 2020, **10**, 2001997.
13. M. Chen, W. Zhu, H. Guo, Z. Tian, L. Zhang, J. Wang, T. Liu, F. Lai and J. Huang, *Energy Storage. Mater.*, 2023, **59**, 102760.
14. L. Ma, G. Zhu, Z. Wang, A. Zhu, K. Wu, B. Peng, J. Xu, D. Wang and Z. Jin, *Nano Lett.*, 2023, **23**, 5272-5280.
15. J. J. Hong, L. Zhu, C. Chen, L. Tang, H. Jiang, B. Jin, T. C. Gallagher, Q. Guo, C. Fang and X. Ji, *Angew. Chem. Int. Ed.,* 2019, **58**, 15910-15915.